Neutron- and x-ray-scattering study of the two length scales in the critical fluctuations of $SrTiO_3$

K. Hirota,* J. P. Hill, S. M. Shapiro, and G. Shirane
Department of Physics, Brookhaven National Laboratory, Upton, New York 11973

Y. Fujii
Institute for Solid State Physics, The University of Tokyo, Minato-ku, Tokyo 106, Japan
(Received 2 May 1995)

Combined high-resolution neutron and x-ray diffraction experiments have been performed on several differently prepared single crystals of $SrTiO_3$ in order to investigate the two length scales present near the cubic-to-tetragonal phase transition occurring at $T_c \sim 100$ K. The x-ray measurements show that the narrow component (long-length scale) exists in all crystals. However, the broad component (short-length scale) is sample dependent and unobservable in some crystals. The neutron experiments, which probe the entire sample volume, reveal that the narrow component is present only in thinly sliced samples (thickness <1 mm), whereas bulk samples show only the broad component. In the thinly sliced samples, the broad component is not observed. These results lead to the conclusion that the narrow component is located in the near surface, or "skin," region of the crystal and the size of the skin is sample dependent. By using the energy analysis capabilities of the neutron experiment we could separate the soft mode from the elastic central peak and found that the intensity of the central component is sample dependent, which is consistent with theories relating the origin of the central component to defects.

I. INTRODUCTION

The cubic-to-tetragonal transition of the perovskite $SrTiO_3$ is driven by the instability of a zone-boundary (R point$=\frac{1}{2}\frac{1}{2}\frac{1}{2}$) phonon mode with a frequency ω_∞ that approaches zero as the temperature decreases to the transition temperature $T_c \approx 100$ K.[1,2] It is considered a prototypical system which has confirmed the soft-mode theory of structural phase transitions.[3,4] In 1971, Riste *et al.*[5] discovered an unexpected "central peak" in a neutron-scattering study of the soft-phonon mode in $SrTiO_3$. As shown in Fig. 1(a), the central peak appears at energy $\omega=0$ at an R point and its intensity diverges at T_c.[6] Although the central peak has been thoroughly studied and also is present in many other systems, e.g., $KMnF_3$,[7] $LaAlO_3$,[8] and Nb_3Sn,[9] there does not yet exist a comprehensive explanation of its origin. However, the elastic nature of the central peak and some other evidence[10,11] favor a defect origin, which ascribes the elasticity to a long time trap of soft phonons at defects,[12] rather than a dynamical origin due to anharmonic processes.[13]

In 1986, Andrews[14] observed in $SrTiO_3$ an anomalous two-component q profile in an x-ray critical scattering; an unexpected narrow peak in addition to the usual broad one. This implies the existence of a second, and much larger, length scale, and is contrary to our understanding of critical phenomena, where a single correlation length is expected to characterize the average size of the fluctuating regions above T_c. McMorrow *et al.*[15] used synchrotron radiation to study the temperature dependence and anisotropy of the two length scales [see Fig. 1(b)]: The broad component has a Lorentzian character with an anisotropy in q space, whereas the narrow component, or *quasi*-Bragg peak, is well described with an isotropic Lorentzian-squared line shape. This phenomenon has been studied intensively, not only in $SrTiO_3$ but also other perovskites,[16] and some rare-earth metals,[17,18] where similar phenomena are observed in the magnetic critical fluctuations above the antiferromagnetic transition. One of the most important results is the spatial distribution of the narrow component determined in Tb. Gehring *et al.*[19] and Hirota *et al.*[20] used a particular (narrow beam and small angle) scattering geometry in a neutron-diffraction experiment to establish that the narrow component originates in the near-surface volume or "skin" of the Tb crystal. Note that here the term "skin" refers not just to the surface, but a more extended near-surface volume. The narrow component is spread over an order of hundred microns and not just one or two. Gehring *et al.*[21] have recently reported a complete absence of the narrow component in the bulk.

In order to elucidate the relationship between the narrow, quasi-Bragg component observed in the x-ray experiments, and the central peak in the neutron-scattering studies, Shirane *et al.*[22] performed a detailed study of the q dependence of the central peak in the inelastic neutron-scattering spectrum of $SrTiO_3$. They have shown that the central peak and the quasi-Bragg peak are distinct entities. It is a combination of the central peak and the soft phonon that gives rise to the anisotropic broad component observed in the x-ray measurements. Despite an intensive search with a q resolution comparable to the width of the narrow component, they failed to observe the sharp feature in their bulk single crystal [see Fig. 1(c)]. As a possible explanation of this absence, they pointed to the difference between the penetration depth of neutrons and x rays. Typical x-ray energies used for studying the two length scales of $SrTiO_3$ (8–17 keV) probe crystals to depths of the order of several μm, whereas neutrons detect the scattering from the entire volume of the sample. If

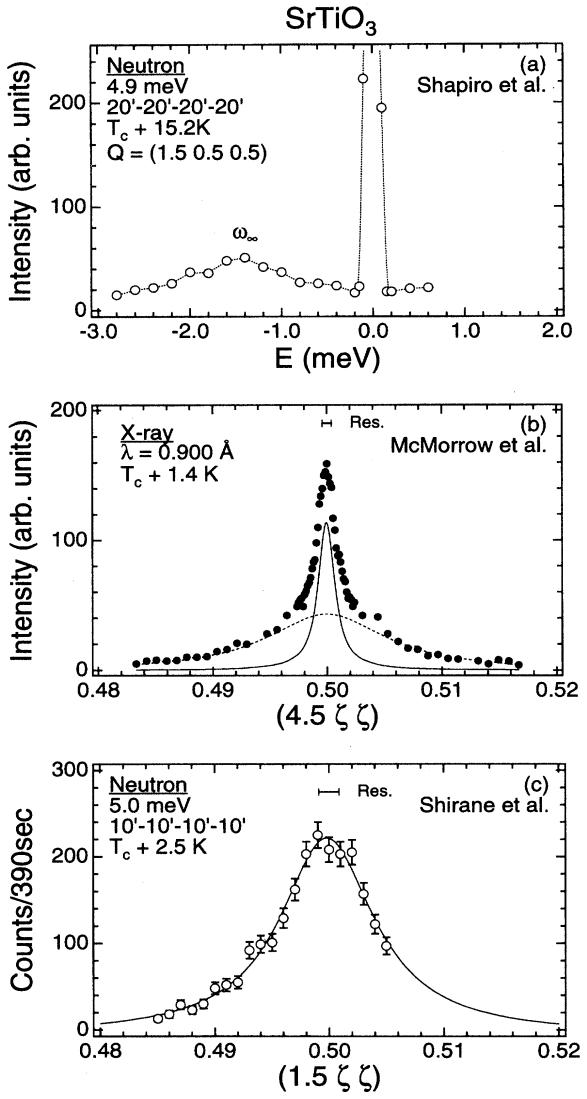

FIG. 1. (a) Inelastic neutron-scattering spectrum of $SrTiO_3$ at $T_c+15.2$ K measured by Shapiro *et al.* (Ref. 6) which clearly reveals the central component as well as the soft phonon. (b) Typical x-ray profile of McMorrow *et al.* (Ref. 15) showing the two length scales. The solid and dotted curves correspond to Lorentzian squared and Lorentzian line shape to the narrow and broad components, respectively. (c) High-resolution elastic neutron diffraction scan at (3/2 1/2 1/2) of Shirane *et al.* (Ref. 22). The solid curve is a fit to a Lorentzian.

the narrow component originates in the near-surface region of the sample, as is the case for Tb, then the sharp quasi-Bragg peak in the neutron scattering may remain unobservable due to the dominance of the broad component originating in the bulk.

In order to study the role of the near-surface region, we have investigated thin slices of $SrTiO_3$ crystals of different thicknesses (0.5–2 mm) and three bulk crystals, one of which was used in the study of Shirane *et al.*[22] as mentioned above and also by Shapiro *et al.*[6] in their earlier work. A combination of x-ray and neutron-scattering techniques was utilized. We begin in Sec. II by summarizing the samples and the experimental procedures. In Sec. III, the temperature dependence of basic parameters around the cubic-to-tetragonal transition is shown in order to demonstrate an accurate determination of T_c, and x-ray studies of the two length scales are presented. Section IV A provides the salient result of the present experiment, i.e., the observation of the narrow component in the thin-sliced samples in the neutron-scattering experiment. The temperature and q dependence of the central component and the soft phonon in the two bulk crystals are described in Sec. IV B. The paper concludes with discussions and a summary in Sec. V.

II. EXPERIMENTAL DETAILS

A. Samples

We used a total of seven samples, among which six were used for neutron-scattering measurements and three were studied by x-ray scattering. These were supplied by three different commercial sources: Sanders Associates (SA),[23] Atomergic Chemetals Co. (AC),[24] and Earth Jewelry Co. (EJ).[25] We denote each sample with a combination of the providing company's name and its thickness, e.g.," AC-1.0" for a 1.0 mm thickness crystal from Atomergic Chemetals Co. and "SA-bulk" for a bulk crystal from Sanders Associates.

SA-bulk was made more than two decades ago. It was grown by the top-seeded method, which yielded an essentially strain-free crystal with an effective mosaic spread of 0.017° from x-ray diffraction and 0.004° from γ-ray diffraction.[26] The crystal is transparent but has a brownish color whose origin is not completely understood. Darlington and O'Connor[27] speculated that iron impurities, which were detected as weak Fe $K\alpha$ fluorescent radiation, may yield a brownish color to their specimen after a heat treatment, during which the oxidation state of the iron could be changed. SA-bulk has been extensively studied with neutron scattering.[6,22]

Recently, $SrTiO_3$ has become widely used as a substrate for high-T_c superconducting thin films. Consequently, high and uniform quality samples are now commercially available. Both AC and EJ provide single crystals grown by the Verneuil method which has been greatly improved in recent years. These crystals are almost equal to SA-bulk in their quality as determined by the mosaic. However, unlike SA-bulk, these modern $SrTiO_3$ crystals are clear, with no brownish tint. All the modern crystals studied have shiny flat (100) and (011) surfaces produced by so-called "mechanochemical" polishing with an alkaline solution containing colloidal silica particles. It is shown by the atomic force microscopy that the surface thus prepared has only small corrugations of 0.2–0.8 nm and is as smooth as that of an ordinary Si wafer,[28] indicating that this treatment yields minimum damages to the surface. In order to eliminate the effects of strain due to mounting, each sample was first placed in an aluminum case (with a window if used for x-ray studies) then attached to a copper (x-ray) or aluminum (neutron) block. The sample was mounted in a beryllium (x-ray) or aluminum (neutron) can so as to give a crystallographic (hkk) zone. The sample can was filled with helium gas to improve heat transfer and attached to the cold finger of a

TABLE I. Specifications of the samples studied. N and X indicate that the sample was studied with neutron or x-ray scattering, respectively. Mosaic is full width at half maximum (FWHM) of a θ scan at the (200) peak above T_c as measured by x ray. Mosaic in parentheses indicates the value measured by neutron for $E_i=5.0$ meV with 20′-20′-20′-20′ [after collecting the slices together for AC-0.5(×9) and EJ-2.0(×3)]. The effective volume was estimated using "standard" phonons at (5/2 1/2 1/2) for $E_i=14.7$ meV with 20′-20′-20′-20′ at T_c+20 K and at (3/2 1/2 1/2) for $E_i=5.0$ meV with 40′-20′-40′-20′ at T_c+15 K.

Name	Size (mm^3)	Experiment	Mosaic (°)		Effective volume	Notes
SA-bulk	10×10×10	N, X	0.017	(0.20)	1.0	Brownish
AC-bulk	15×15×15	N		(0.20)	2.63	
EJ-bulk	10×10×20	N	~0.03	(0.20)	1.25	
AC-0.5(×9)	15×15×0.5	N, X	0.020	(0.34)	0.80	
AC-1.0	10×10×1	N		(0.21)	0.16	
EJ-0.5	10×10×0.5	X	0.025			
EJ-2.0(×3)	15×15×2	N	~0.03	(0.25)	1.18	

closed-cycle He cryostat. The lattice parameter at room temperature is 3.91 Å. Detailed specifications of the samples are provided in Table I.

B. X-ray scattering

X-ray scattering experiments were performed at Brookhaven National Laboratory's (BNL) National Synchrotron Light Source, on the beam lines X22C and X22B. X22C employs a nickel mirror to cut off the incident energy above 11.5 keV, a tunable double-crystal Ge(111) monochromator, and a Ge(111) analyzer in the vertical scattering geometry. X22B uses a nickel mirror and a single flat Ge(111) monochromator and a Ge(111) analyzer in the horizontal scattering geometry. These configurations leave practically no $\lambda/2$ contamination for an incident energy higher than 5.8 keV. Each monochromator was adjusted so as to give the wave length of 1.54 Å ($E=8.05$ keV). For the triple-axis configurations, the q resolution along [100] and [011] directions at the (5/2 1/2 1/2) R point were 0.0006 and 0.0003 Å^{-1} half width at half maximum (HWHM) with a Lorentzian-squared line shape for X22C, and 0.0010 and 0.0007 Å^{-1} HWHM in a Lorentzian line shape for X22B. These values were estimated from the superlattice Bragg peak in the low-temperature phase. The difference between the line shapes arises from the different monochromator in each spectrometer. The resolution perpendicular to the scattering plane was about 0.01 Å^{-1} HWHM for both spectrometers. We also used a double-axis (no analyzer) configuration on X22C, in which the q resolution along [100] and [011] directions were 0.0028 and 0.0009 Å^{-1} HWHM.

C. Neutron scattering

The neutron-scattering measurements were carried out on the triple-axis spectrometer H8 located at the High Flux Beam Reactor at BNL. The spectrometer was set up in a standard triple-axis mode using incident energy $E_i=14.7$ meV (wave length $k_i=2.67$ Å^{-1}) or 5 meV ($k_i=1.55$ Å^{-1}), typically with a collimation 20′-20′-sample-20′-20′. The (002) reflection of pyrolytic graphite (PG) was used to monochromate the neutron beam, together with either two PG filters or a Be filter to eliminate higher-order contamination from the incident beam. We also utilized PG (002) for an analyzer. At $E_i=14.7$ meV with 20′-20′-20′-20′, the q resolution along [100] and [011] directions at (5/2 1/2 1/2) are 0.011 and 0.007 Å^{-1} HWHM. The q resolution decreases to 0.004 Å^{-1} HWHM along both [100] and [011] at (3/2 1/2 1/2) at $E_i=5.0$ meV with 20′-20′-20′-20′. The line shape of the resolution in the scattering plane approximates a Gaussian function. The vertical resolution is estimated at about 0.03 – 0.04 Å^{-1} HWHM.

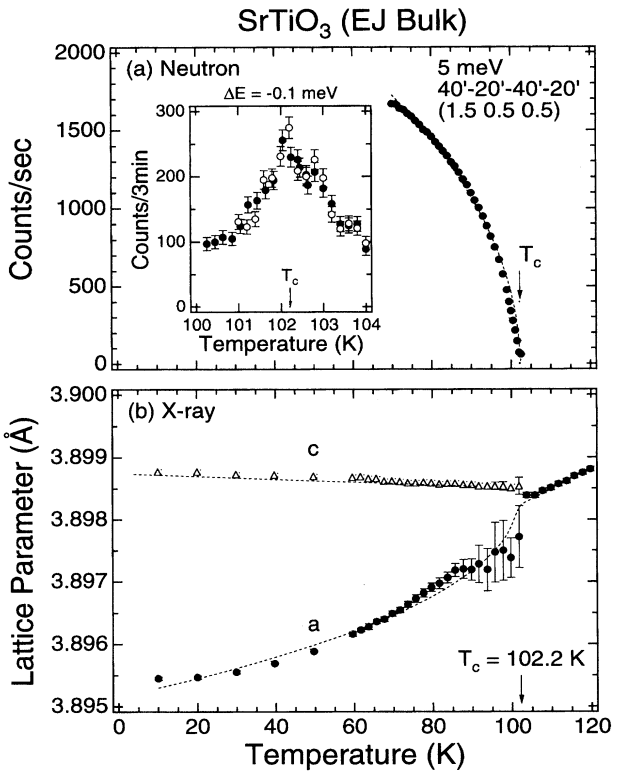

FIG. 2. (a) The temperature dependence of the superlattice intensity at (3/2 1/2 1/2), as measured by neutron scattering. The inset shows the superlattice intensity at a small energy transfer ($\Delta E=-0.1$ meV) in the vicinity of T_c. The open and filled circles correspond to data taken on cooling and heating, respectively. (b) The lattice constant as measured by x-ray scattering at the (300) Bragg peak. The peak profiles are fitted with double and single Lorentzian-squared functions below and above T_c.

In order to compare scattering intensities from different samples, we need to normalize the intensities with the volume of each sample. The volume calculated from the physical size, however, may not be appropriate because a different part of the sample may have a different scattering intensity due to absorption, extinction, and nonuniformity of the neutron beam. Instead, we utilized the integrated intensity of the R point phonon, measured under the same experimental conditions for each sample, to normalize the volumes. We measured the soft phonon at (5/2 1/2 1/2) for $E_i = 14.7$ meV with 20′-20′-20′-20′ at $T_c + 20$ K and at (3/2 1/2 1/2) for $E_i = 5.0$ meV with 40′-20′-40′-20′ at $T_c + 15$ K. The values of volumes normalized to SA-bulk are summarized in Table I.

III. ORDER PARAMETERS AND TWO LENGTH SCALES

A. Cubic-to-tetragonal transition at T_c

Figure 2(a) shows the temperature dependence of the superlattice peak intensity at (3/2 1/2 1/2) of EJ-bulk, as measured by neutron scattering. As already known, the order parameter shows continuous behavior with temperature and no observable thermal hysteresis, confirming the truly second-order nature of the transition.[29] T_c was determined by setting the spectrometer at a superlattice reflection and offsetting the energy by a small amount ΔE from $E = 0$. Since the critical scattering due to the softening of a zone-boundary phonon mode reaches its maximum at T_c, measuring the maximum in the temperature dependence of the intensity for several ΔE and extrapolating them to $\Delta E = 0$ determines T_c. [See inset of Fig. 2(a).] A similar technique can be applied for x-ray scattering measurements, where the scattering vector is offset from the R point by a small amount. We indeed observed a distinct peak on the temperature dependence of the intensity for AC-0.5 by x-ray scattering. As we will show in the next subsection, however, the critical scattering, i.e., the broad component, does not appear in the x-ray scattering of the other two samples, SA-bulk and EJ-0.5. In those cases, we estimated T_c by monitoring the width of the narrow component and the lattice constant. T_c's determined by these methods agree well with each other. Figure 2(b) shows the temperature dependence of the lattice parameter of EJ-bulk, as measured by x-ray scattering.

B. X-ray measurements of two length scales

Typical x-ray scattering profiles exhibiting two length scales are shown in Figs. 3(a)–(d), obtained in AC-0.5 along with the [100] and [011] directions at (5/2 1/2 1/2) on X22C without using an analyzer. As pointed out by Gibaud *et al.*[30] and Thurston *et al.*,[17] the broad component is more easily detected with a larger resolution volume. The q resolution of the double-axis mode employed is good enough to separate the narrow component from the broad one. For comparison, we also tried the triple-axis mode for the same sample and confirmed that the relative intensity of the broad component against the narrow component decreases. In order to obtain the temperature dependence of the intensity and inverse correlation length κ, we performed a least-squares fitting of several models convolved with the appropriate resolution function. To speed the computations, we performed the convolution over the out-of-plane resolution function analytically assuming that it is approximately triangular. Results of the convolution of a Lorentzian and Lorentzian-squared functions with a triangular function are given in the Appendix. The data are well described by a Lorentzian-squared cross section for the narrow component and a Lorentzian cross section for the broad component, as shown in Fig. 3. McMorrow *et al.*[15] pointed out that the narrow component cross section is almost isotropic in the scattering plane, while the broad component is ~36% wider in the [011] direction than in [100]. This is consistent with our results.

Figures 3(e) and 3(f) show peak profiles for EJ-0.5 along with the [011] direction at (5/2 1/2 1/2) without an analyzer. Although these data were taken under exactly same experimental conditions as used for AC-0.5, we did not find any sign of the broad component despite extensive investigations. This suggests that the broad component is very weak

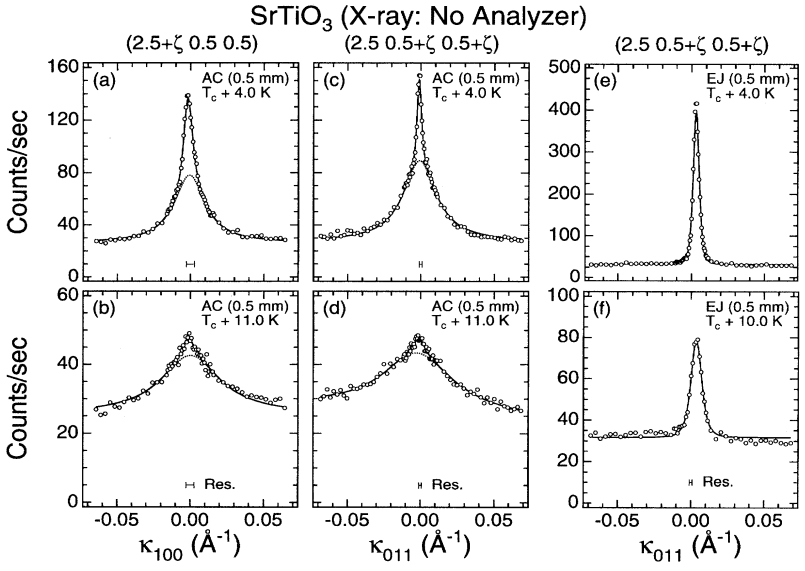

FIG. 3. X-ray diffraction peak profiles at (5/2 1/2 1/2) in the double-axis mode. The resolution was measured slightly below T_c, where the tetragonal distortion is negligible. The solid and dotted curves are fits to Lorentzian squared plus Lorentzian and single Lorentzian functions, convolved with the resolution function.

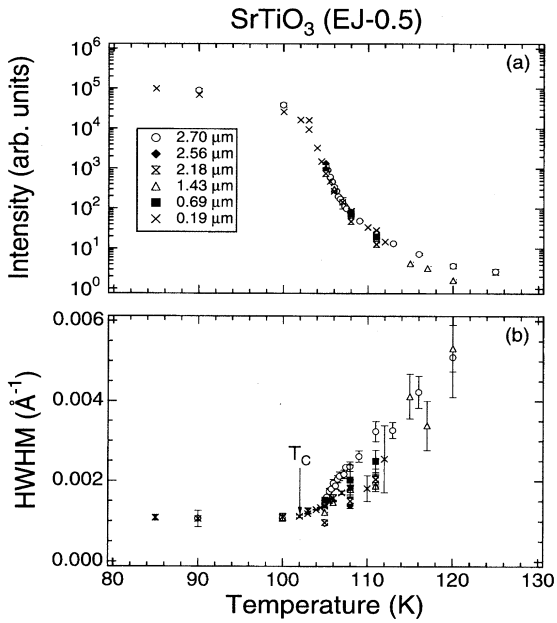

FIG. 4. (a) The temperature dependence of the intensity for AC-0.5 at different penetration depths, which are estimated using Eqs. (1) and (2). The intensities are normalized using the data below 100 K. (b) The temperature dependence of the HWHM of the peak along the [100] direction.

or absent in this sample. In addition, we studied the depth dependence of the narrow component in AC-0.5 by changing the incident angle α and the exit angle β while keeping the scattering vector $\mathbf{Q}$ at the same position. This is equivalent to an azimuthal scan, in which the rotation angle Ψ of a reference vector is varied about $\mathbf{Q}$, with Ψ defined to be zero when the reference vector is in the scattering plane. Suppose the reference vector is chosen to be the surface normal, e.g., [011] for EJ-0.5, the surface normal will be rotated into the plane defined by $\mathbf{Q}$ and the diffractometer axis (θ-2θ axis) so that, for Ψ equal to 90°, the incident angle α will equal the exit angle β. From a geometrical consideration, the penetration depth Λ_d is given as follows:

$$\Lambda_d = L \Big/ \left[\frac{1}{\sin(\theta_B+\eta)} + \frac{1}{\sin(\theta_B-\eta)} \right], \tag{1}$$

$$\eta = \tan^{-1}[\sin(90^\circ - \Psi)\tan\chi], \tag{2}$$

where L is the absorption length ($L=16.4$ μm at $\lambda=1.54$ Å^{-1} for $SrTiO_3$), θ_B is the Bragg angle [19.21° at (3/2 1/2 1/2)], and χ is the angle between the reference vector and the scattering vector when $\Psi=0$. α and β are given by $\theta_B+\eta$ and $\theta_B-\eta$, both of which must be larger than zero to have a finite penetration depth. At the (3/2 1/2 1/2) R point, we could continuously adjust the penetration depth between 2.7 μm at $\Psi=90°$ and 0 μm at $\Psi>99.3°$. As shown in Fig. 4, we found no depth dependence in the temperature dependence of the normalized intensity and the inverse correlation length κ. These findings are compatible with our current understanding that the narrow component is located in the near-surface or "skin" region, if one assumes that the thickness of the skin varies from sample to sample. Namely, the skin region, which primarily provides the narrow component, of EJ-0.5 is thicker than 3 μm, while AC-0.5 has thinner skin so that x rays can penetrate to the region of bulk behavior, where the broad component is dominant. The weakness or absence of the broad component in the skin region of EJ-0.5 implies that the lattice dynamics in the skin is different from that in the bulk because the broad component is ascribed to the energy integration of the soft-mode phonon and of the central peak. This important point will require further experimental investigations. We also studied SA-bulk. Similarly, we saw only the narrow component and observed no broad component in this sample, while the neutron-scattering studies show only the broad component even though a q resolution comparable to the narrow component was used. As already mentioned in Sec. I, this difference can also be understood by the concept of the skin region and the difference between the penetration depth of neutrons (~ 1 cm) and that of x rays (~ 1 μm). Very recently, utilizing 100 keV synchrotron radiation, Neumann *et al.*[31] reported that the bulk critical scattering does not exhibit a narrow component, whereas two length scales were observed in the near-surface region in their high q-resolution x-ray diffraction. With a very short wave length as well as a large penetration depth provided at this high energy, they have succeeded in reaching a configuration similar to that used in Tb,[19–21] in which both high q and high spatial resolution are accomplished. Their results are consistent with our conclusions.

The results of the fits to the data for the narrow component are summarized in Figs. 5(a) and 5(b). The integrated intensity of the narrow component is normalized to 100 at T_c. The integrated intensity of the broad component for AC-0.5 is shown with the same normalization as that used for the narrow component of the same sample. It is immediately apparent that the temperature dependence of κ of the narrow component falls on a universal curve regardless of sample, whereas the integrated intensity shows a clear sample dependence. This indicates that there exists a common *nontrivial* mechanism giving rise to the narrow component in the skin region, though the skin thickness may vary from one sample to another. Darlington and O'Connor in their x-ray study found a similar sample dependence in the superlattice peak intensity above T_c.[27] They stated that the scattered intensity falls more rapidly to zero with increasing temperature after annealing the sample at 1000 °C for 24 h and cooling slowly to room temperature over 8 h. They speculated that the annealing reduced the density of dislocations, which are nucleating the low-temperature phase in the surface region at temperatures above T_c of the bulk, and hence contributing to the critical scattering intensity. Note that they published the results in 1976, 10 years before the narrow component was reported by Andrews.[14] Andrews reported that a chemically etched surface shows a much faster fall in the integrated intensity at an R point than a mechanically polished surface. He ascribed this difference to a reduction of the surface damage by chemical etching.

IV. NEUTRON-SCATTERING EXPERIMENTS

A. Observation of the narrow component

From all the findings so far collected, it is reasonable to assume that the narrow component in $SrTiO_3$ is located in

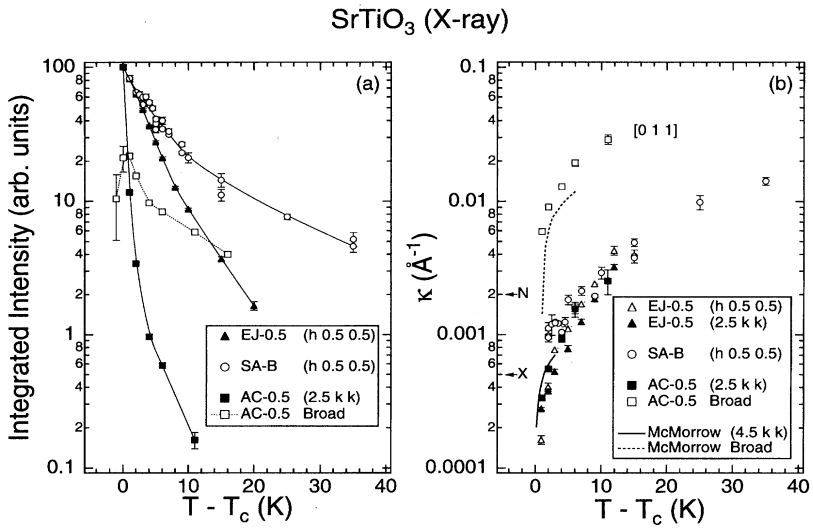

FIG. 5. (a) The temperature dependence of the intensity, obtained from a fitting analysis of x-ray data including a convolution of resolution. The broad component was seen only in AC-0.5, for which the integrated intensity peaks at T_c. (b) The temperature dependence of the inverse correlation length κ, obtained from the same fits as (a). κ of the broad component is along the [011] direction. N and X indicate typical resolution width (HWHM) of neutron and x-ray scattering experiments, respectively.

the near-surface or "skin" region as is the case for Tb. It is, however, still very important to actually observe the narrow component in $SrTiO_3$ by neutron scattering to establish the concept of the skin region. In Tb, one isolates the scattering from the skin region by utilizing a very narrow beam together with the small scattering angle ($\theta = 1.35°$), which allows the neutron beam to be nearly parallel to the flat surface.[19–21] This technique cannot be used for $SrTiO_3$ because of the large scattering angle at the R point. Instead, we took the following approach: Since the scattered intensity is proportional to the effective volume of the scatterer, we can increase the total volume of the skin and therefore the intensity of the narrow component by cutting a bulk sample into many slices and stacking them together. To avoid an increase of the mosaic during the process, the sample was carefully cut into nine 0.5 mm slices and placed in an aluminum box in the original order (AC-0.5×9) after mechanochemical polishing of the surfaces as described in Sec. II A. The effective mosaic increased by about 30%, which is still small enough to measure the width of the narrow component. In order to investigate thickness dependences, we also studied AC-1.0 and EJ-2.0×3 as well as bulk samples.

Figures 6(a) and 6(b) show the q scans for SA-bulk and AC-1.0 taken under the same experimental conditions, i.e., $E_i = 5.0$ meV with 20′-20′-20′-20′ at $T_c + 7.8$ K. Figures 6(c) and 6(d) show peak profiles of SA-bulk and AC-0.5 ×9 with a coarser resolution ($E_i = 14.7$ meV with 20′-20′-20′-20′) and at a higher temperature, $\sim T_c + 40$ K. The intensity is normalized by the effective volume (see Table I) for each sample. These results clearly indicate the presence of the narrow component in the 0.5 and 1.0 mm thick samples. It is uncertain whether these spectra contain the broad component as well as the narrow one. Within counting statistics, there is no clear difference in the quality of fit to a single Lorentzian squared with which a flat background is used, or a broad Lorentzian background is added. The 2.0 mm thick sample (EJ-2.0×3) as well as bulk samples show only the broad component as seen in SA-bulk.

The fitting parameters obtained after deconvolution of the appropriate resolution function are summarized in Figs. 7(a) and 7(b). The dotted lines labeled with κ_L and κ_{L2} correspond to the temperature dependence of the inverse correlation lengths for the broad and narrow components measured by x-ray scattering. κ_c is the HWHM of the peak profile calculated from the renormalized q-dependent soft-mode frequency $\omega_0(\mathbf{q}, T)$. The inverse correlation lengths of the broad component obtained from the neutron-scattering data are consistent both with the x-ray scattering results and the values calculated from the q-dependent phonon frequency.

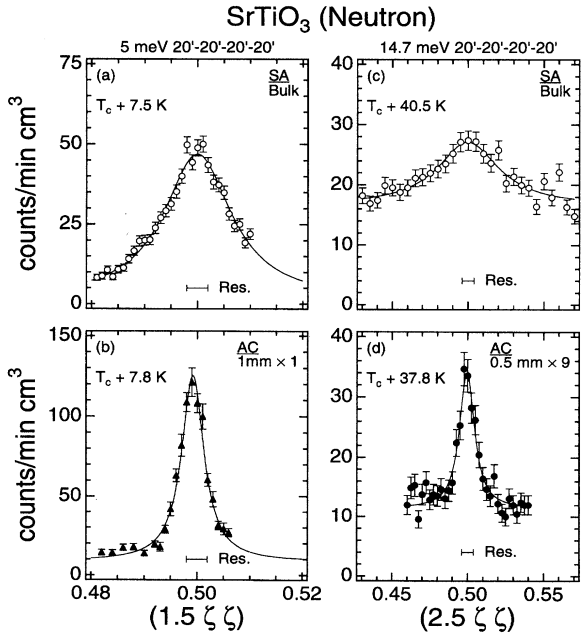

FIG. 6. Neutron-diffraction peak profiles for SA-bulk and thin AC crystals. To avoid artifact due to a deconvolution process, data were taken under identical conditions for a spectrometer configurations and temperatures. Comparison between (a) and (b), and between (c) and (d) indicates the narrow component in the thin AC crystals.

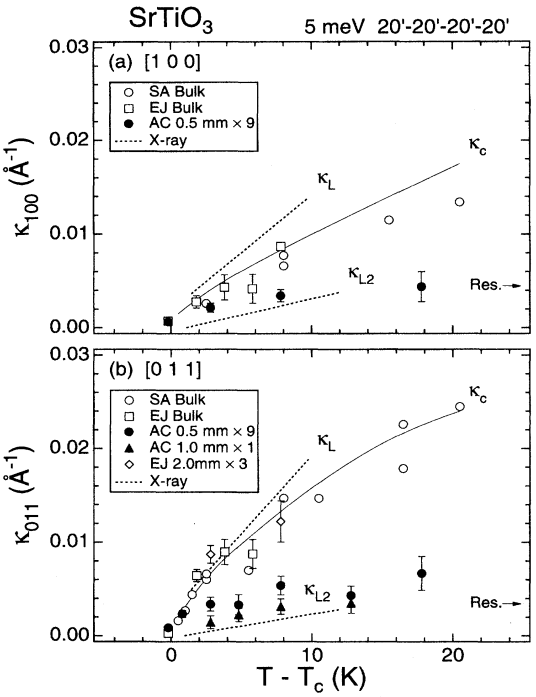

FIG. 7. The temperature dependence of the inverse correlation length κ, obtained from fitting of neutron data taking into account a convolution of resolution. κ_L and κ_{L2} represent the inverse correlation lengths for the broad and narrow components obtained from x-ray measurements. κ_c is calculated from the soft-mode frequencies using Eq. (7), as described in the text.

B. Broad or central component

In the following, we briefly describe the relation between the q-dependent phonon frequency at an R point and the inverse correlation length. The total energy-integrated intensity corresponding to the broad component consists of a central peak part and a soft-mode phonon part: $\int S_{\rm tot}(\mathbf{q},\omega)d\omega=\int[S_{\rm cent}(\mathbf{q},\omega)+S_{\rm phon}(\mathbf{q},\omega)]d\omega$. In the high-temperature limit $k_BT\gg\hbar\omega_\infty(T)$, where ω_∞ is the bare soft-mode frequency, Shapiro *et al.*[6] showed that the equation for the total energy-integrated intensity becomes

$$\frac{T}{\omega_0^2(\mathbf{q},T)}=\frac{T\delta^2}{\omega_0^2(\mathbf{q},T)\omega_\infty^2(\mathbf{q},T)}+\frac{T}{\omega_\infty^2(\mathbf{q},T)}, \tag{3}$$

where δ^2 is a coupling constant of the soft-mode frequency $\omega_\infty(\mathbf{q},T)$ to some postulated relaxing degree of freedom, which gives rise to the central peak. The renormalized phonon frequency $\omega_0(\mathbf{q},T)$ for the total intensity is given by

$$\omega_0^2(\mathbf{q},T)=\omega_\infty^2(\mathbf{q},T)-\delta^2. \tag{4}$$

The temperature and q dependence of the soft-mode frequency $\omega_\infty(\mathbf{q},T)$ as well as those of the coupling constant δ were extensively studied for SA-bulk by Shapiro *et al.*[6] and Shirane *et al.*[22] It was found that $\omega_\infty(\mathbf{q},T)$ has a dispersion curve that may be written as

$$\omega_\infty^2(\mathbf{q},T)=\omega_\infty^2(0,T)+\alpha_q q^2, \tag{5}$$

where $q=0$ corresponds to an R point and α_q is the slope of the dispersion curve along a particular direction. Shirane *et al.*[22] obtained $\alpha_{[100]}=3160$ meV^2 Å^2 and $\alpha_{[011]}=1000$ meV^2 Å^2. The integrated phonon intensity $I_\infty(\mathbf{q},T)=\int S_{\rm phon}(\mathbf{q},\omega)d\omega$ is given by

$$I_\infty(\mathbf{q},T)=\frac{T}{\omega_\infty^2(0,T)+\alpha_q q^2}=\frac{T/\alpha_q}{\kappa_\infty^2+q^2}, \tag{6}$$

where the inverse correlation length for phonon is $\kappa_\infty^2=\omega_\infty^2(0,T)/\alpha_q$. With the assumption that the coupling constant δ^2 is q independent, then the inverse correlation length for the total scattering $I_0(\mathbf{q},T)=\int S_{\rm tot}(\mathbf{q},\omega)d\omega$ can similarly be defined as $\kappa_0^2=\omega_0^2(0,T)/\alpha_q$. Using κ_∞^2 and κ_0^2, we can obtain the integrated intensity for the central peak as the difference between $I_0(\mathbf{q},T)$ and $I_\infty(\mathbf{q},T)$,

$$I_{\rm cent}=\frac{T}{\alpha_q}\left(\frac{1}{\kappa_0^2+q^2}-\frac{1}{\kappa_\infty^2+q^2}\right)=\frac{T}{\alpha_q^2}\left[\frac{\delta^2}{(\kappa_0^2+q^2)(\kappa_\infty^2+q^2)}\right]. \tag{7}$$

At high temperatures where $\omega_\infty^2\gg\delta^2$ and thus $\omega_0^2\approx\omega_\infty^2$, Eq. (7) becomes a Lorentzian squared,

$$I_{\rm cent}=\frac{T}{\alpha_q^2}\frac{\delta^2}{(\kappa_0^2+q^2)^2}. \tag{8}$$

The HWHM of this central peak line shape is $\kappa_c=\sqrt{\sqrt{2}-1}\times\kappa_0$. As mentioned in Ref. 22, it is difficult to distinguish between Lorentzian and Lorentzian-squared line shapes for the central peak, $I_{\rm cent}(\mathbf{q},T)$, because the major difference is in the tails of the line shape, where the count rate is low and the statistics are inevitably poor.

The soft-mode behavior of bulk $SrTiO_3$ has been extensively studied.[6,22] We extended the measurements to the other samples of our study in order to probe any sample dependence of the soft phonon. We performed energy scans at various momentum transfers along the [100] direction from an R point for a number of temperatures. We assumed a dispersion surface described by Eq. (5), for which the scattering function may be written as

$$S(Q,\omega)=C_0(N+\tfrac{1}{2}\mp\tfrac{1}{2})e^{-2W(Q)}\frac{|\mathbf{Q}\cdot\mathbf{e}|^2}{\hbar\omega_\infty(\mathbf{q})}\delta[\omega\pm\omega_\infty(\mathbf{q})]\times\delta(\mathbf{Q}-\mathbf{G}-\mathbf{q}), \tag{9}$$

where N is the Bose-Einstein factor $N=\{\exp[\hbar\omega_\infty(\mathbf{q})/kT]-1\}^{-1}$, $\mathbf{e}$ is the phonon polarization vector, and $\mathbf{G}$, in this case, is an R point. If we allow for damping of the phonon,

$$S(Q,\omega)\approx\frac{CQ^2}{\hbar\omega_\infty(\mathbf{q})}e^{-2W(Q)}\left\{\frac{N+1}{1+\left[\frac{\omega-\omega_\infty(\mathbf{q})}{\Gamma}\right]^2}+\frac{N}{1+\left[\frac{\omega+\omega_\infty(\mathbf{q})}{\Gamma}\right]^2}\right\}. \tag{10}$$

The δ function is replaced with a Lorentzian line shape with the damping factor Γ in our approximation. We fitted a series of energy scans with different $\mathbf{q}$ at the same temperature with

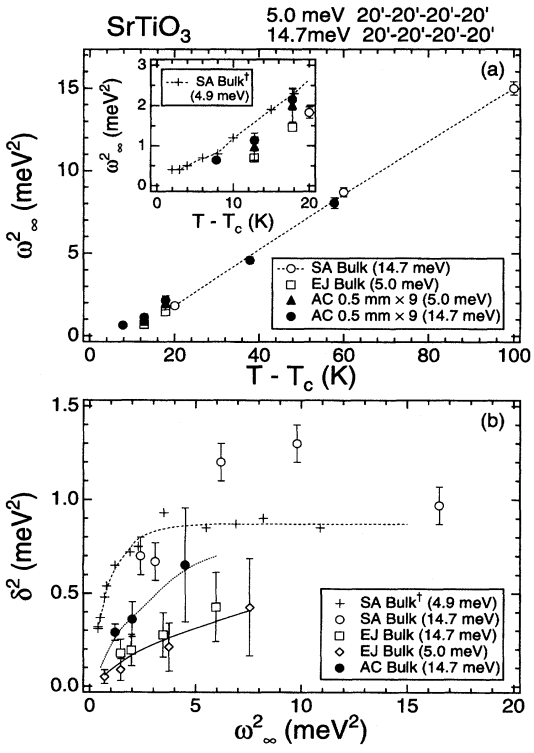

FIG. 8. (a) The temperature dependence of the soft-mode frequency ω_∞^2. The dotted line and data points for SA-bulk at $E=4.9$ meV are from Ref. 6. The inset shows the temperature dependence in the vicinity of T_c. (b) The coupling constant between the soft-mode phonon and the central peak, $\delta(\mathbf{q},T)$, is plotted as a function of the soft-mode frequency $\omega_\infty^2(\mathbf{q},T)$. Data for SA-bulk at $E=4.9$ meV is taken from Ref. 22. Curves are guides for the eye.

the scattering function described with Eqs. (5) and (10) convolved with the resolution function. Thus, the phonon frequency at the R point, $\omega_\infty^2(0,T)$, and the slope of the soft-mode frequency along the [100] direction, $\alpha_{[100]}$, was obtained. The value for EJ-bulk obtained at T_c+20 K is $\alpha_{[100]}=2940$ meV^2 Å^2, which is consistent with the value for SA-bulk.[6,22] Figure 8(a) shows the temperature dependence of $\omega_\infty^2(0,T)$ for three different samples. All the values fall on a single line, which is approximately described as $\omega_\infty^2(0,T)\approx 0.18(T-T_c)$,[22] and shows that the soft-mode phonon is unaffected by the size of the skin at $(T-T_c)>5$ K.

In Sec. IV A, we assumed that δ^2 was both q and temperature independent. As pointed out in Refs. 11 and 22, these assumptions are no longer valid at small q and for temperature close to T_c. From Eq. (3), we can calculate δ^2 (for temperatures where the central peak and phonon are well separated in energy) as follows:

$$\delta^2(\mathbf{q},T)=\frac{R}{R+1}\omega_\infty^2(\mathbf{q},T), \tag{11}$$

where R is defined as $R\equiv I_{\text{cent}}/I_{\text{phon}}$. If the resolution function does not change the shape during an energy scan, we can obtain R by comparing integrated intensities for the central peak and the phonon without performing deconvolution. We have confirmed that R thus obtained is actually consistent with the value estimated through a rigorous deconvolution. Instead of plotting δ^2 as a function of $\mathbf{q}$ or T, we utilize $\omega_\infty^2(\mathbf{q},T)$ as an independent variable. As shown in Fig. 8(b), δ^2 for each sample falls on its own unique curve regardless of $\mathbf{q}$ and T, indicating that δ^2 is a function of ω_∞^2. The figure shows a clear sample dependence. The central peak is weakest in AC-bulk and strongest in SA-bulk. It seems likely that newly grown AC-bulk contains less defects than SA-bulk, which was grown more than 20 years ago. Perhaps, the brownish color of SA-bulk is related to the defects giving rise to the enhanced δ. This observation is consistent with Refs. 10 and 11, in which a systematic enhancement of the central peak intensity was shown with increasing defect concentration.

V. DISCUSSIONS AND SUMMARY

Now that we have clarified the spatial origin of the narrow component in $SrTiO_3$, let us consider the possible explanation of its *physical* origin. Any theory describing the narrow component has to explain the following established facts: (i) A variety of systems show two length scales near magnetic or structural phase transition. (ii) The narrow component in all of these systems seems to be located in the near-surface region as established in Tb (Refs. 19–21) and $SrTiO_3$. (iii) The temperature dependence of κ of the narrow component is independent of the sample quality. (iv) The sample quality affects the intensity of the narrow component, which is also seen as the absence of the broad component in x-ray scattering measurements of some samples. (v) Considering that a typical penetration depth of 8 keV x rays at the R point (5/2 1/2 1/2) is 3 μm, we can conclude that the skin thickness of $SrTiO_3$ is greater than this and varies with the sample, and that the broad component does not coexist in that region.

The first attempt to understand the physical origin of the narrow component was made by Ryan *et al.*[16] with respect to their x-ray-scattering results on $RbCaF_3$. They referred to a model proposed by Imry and Wortis,[32] in which the influence of quenched impurities on a first-order phase transition is discussed. In this model, the free energy is assumed to be lowered in some regions around impurities, and domains form around a defect center if the cost in interfacial free energy is not too large. They showed that the size l of such domains or, the scale of the phase fluctuations among domains, can be larger than the scale of the coherence length ξ $(=2\pi/\kappa)$ about the local minimum of the free energy in each domain. This theory can qualitatively explain the larger length scale. However, it indicates the coexistence of the narrow and broad components, which is incompatible with our results. Moreover, this theory is specific to first-order transition and requires no inhomogeneous distribution of defects. Thurston *et al.*[18] extended this theory quantitatively, and explained the relation between the critical exponent ν of the narrow component and that of the broad one.

Another theoretical approach can be rooted to the work of Osterman, Mohanty, and Axe,[33] who performed a low-resolution x-ray study of $SrTiO_3$. In order to explain a dependence of the superlattice reflection intensity in $SrTiO_3$ on the x-ray penetration depth, they invoked inhomogeneous

surface strains that couple quadratically to the order parameter and renormalize T_c. The free energy they wrote is

$$F=a(T-T_c)Q^2+BQ^4+DQ^6+\cdots+\gamma Q^2\langle\eta\rangle+\frac{K}{2}\langle\eta^2\rangle$$
$$=a\left(T-T_c+\frac{\gamma\langle\eta\rangle}{a}\right)Q^2+BQ^4+DQ^6+\cdots+\frac{K}{2}\langle\eta^2\rangle, \quad (12)$$

where $\langle\eta\rangle$ indicates an averaged strain due to defects, and Q is the order parameter. $(K/2)\langle\eta^2\rangle$ is the averaged elastic energy and $\gamma Q^2\langle\eta\rangle$ represents the lowest-order nonvanishing coupling term between the strain and the order parameter. $\langle\eta\rangle$ indicates a strain due to defects that is not an order parameter, but may have a spatial dependence. Under such conditions, the surface can order before the bulk with a new characteristic length scale.[34] Axe[35] has extended this idea to more general inhomogeneous strain distributions, and showed that this could give rise to a quasistatic second length with a Lorentzian-squared q dependence. These features are consistent with our observations. Inhomogeneous strain distributions can be explained in terms of the existence of the surface boundary or a higher defect concentration near the surface. Although there are experiments, including the present study, which observed no depth dependence,[36] such an inconsistency can be explained in terms of a variation of the skin thickness from sample to sample. It would be worthwhile to study the depth dependence of the order parameter and of the two length scales in a sample which shows both components in the x-ray scattering data, i.e., for a sample in which the skin thickness is thinner than the x-ray penetration depth.

Recently, Cowley[37] proposed an alternative renormalization in the free energy in the near-surface region. He introduced a *spontaneous* strain, which becomes finite below T_c:

$$F=a(T-T_c)Q^2+BQ^4+DQ^6+\cdots+\gamma Q^2\eta+\frac{K}{2}\eta^2. \quad (13)$$

From the condition $\partial F/\partial\eta=0$, we have $\eta=-(\gamma/K)Q^2$. Therefore,

$$F=a(T-T_c)Q^2+\left(B-\frac{\gamma^2}{2K}\right)Q^4+DQ^6+\cdots. \quad (14)$$

Since the renormalized fourth-order term is smaller than the unrenormalized one, the system becomes closer to a tricritical point (when the fourth-order term is zero), where the critical exponent for the order parameter, β, changes from 1/2 to 1/4 for the Landau theory. Such coupling was recently reported in the inorganic spin-Peierls compound $CuGeO_3$.[38] If the spontaneous strains exist only near the surface, critical phenomena in that region will be different from those in the bulk, and Cowley speculates that this may be caused by surface vibrational modes, thus to be an intrinsic effect.

Although, at present, no theory provides a complete explanation of the two length scales, there is a general agreement that strain fields play a fundamental role. Several attempts to control strain fields have been already made. Watson *et al.*[39] performed x-ray magnetic scattering measurements on a smooth surface of UO_2 and then mechanically roughened the same surface to introduce defects. They observed the narrow component on the roughened surface, but not on the smooth surface. This result is consistent with a model with strain fields. However, it is difficult to relate the result to a specific model for the origin of the strain. It is clearly desirable to establish a method for controlling strains in a reproducible manner, which hopefully would lead to detailed understanding of the physical origin of the second length scale.

In summary, we have established the following in $SrTiO_3$; (i) There exists a "skin" region in which the narrow component is dominant. (ii) The thickness of the skin region, i.e., the effective volume of the narrow component, has a sample dependence. (iii) Temperature dependence of κ of the narrow component is independent of sample. (iv) The soft-mode frequency $\omega_\infty(\mathbf{q},T)$ does not depend on sample, whereas the coupling constant δ of the soft mode to the defect induced central peak is sample dependent.

ACKNOWLEDGMENTS

We are pleased to acknowledge stimulating discussions with J. D. Axe and R. A. Cowley. We are indebted to Doon Gibbs for many discussions and important suggestions in the experiments. We have also benefitted from discussions with P. M. Gehring, A. Gibaud, J. E. Lorenzo, C. F. Majkrzak, D. F. McMorrow, J. R. Schneider, T. R. Thurston, J. M. Tranquada, and G. M. Watson. This work was supported in part by the U.S.-Japan Cooperative Program on Neutron Scattering. Work performed in the Brookhaven National Laboratory was supported by the Division of Materials Research, U.S. Department of Energy under Contract No. DE-AC02-76CH00016.

APPENDIX

In order to correctly estimate the intensity and inverse correlation length from x-ray scattering data, it is necessary to perform a least-squares fitting of a model convolved with the appropriate resolution function. This is, however, often a time-consuming calculation. By approximating the out-of-plane resolution function as a triangle function, we can speed the computations by analytically performing the convolution along the vertical direction.

In the present experiment, we had [100] and [011] in the scattering plane and $[01\bar{1}]$ along the vertical direction. We set the x axis and y axis along the [100] and [011] directions, and the z axis along the $[01\bar{1}]$ direction, respectively. The triangular vertical resolution with W_z FWHM is given by $(1-|q_z/W_z|)$ for $|q_z|<W_z$. The inverse correlation lengths along [100] and [011] are defined $\kappa_{[100]}$ and

$\kappa_{[011]}$. We assume that $\kappa_{[01\Gamma]}$ is equivalent to $\kappa_{[011]}$. χ_B and χ_N denote the peak intensity of the broad (Lorentzian) and narrow (Lorentzian-squared) components, respectively. The following calculations are the Lorentzian cross section and Lorentzian-squared cross section convolved with the triangular vertical resolution function:

$$\int_{-W_z}^{W_z} \frac{\chi_B}{1+\frac{q_x^2}{\kappa_{[100]}^2}+\frac{q_y^2+q_z^2}{\kappa_{[011]}^2}}\left(1-\left|\frac{q_z}{W_z}\right|\right)dq_z = -\frac{\kappa_{[011]}^2\chi_B}{W_z}\ln\left[1+\left(\frac{W_z}{\kappa_{[011]}}\right)^2\frac{1}{1+\left(\frac{q_x}{\kappa_{[100]}}\right)^2+\left(\frac{q_y}{\kappa_{[011]}}\right)^2}\right] + \frac{2\kappa_{[011]}\chi_B}{\sqrt{1+\left(\frac{q_x}{\kappa_{[100]}}\right)^2+\left(\frac{q_y}{\kappa_{[011]}}\right)^2}}\tan^{-1}\left[\frac{W_z}{\kappa_{[011]}}\frac{1}{\sqrt{1+\left(\frac{q_x}{\kappa_{[100]}}\right)^2+\left(\frac{q_y}{\kappa_{[011]}}\right)^2}}\right], \tag{A1}$$

$$\int_{-W_z}^{W_z} \frac{\chi_N}{\left(1+\frac{q_x^2}{\kappa_{[100]}^2}+\frac{q_y^2+q_z^2}{\kappa_{[011]}^2}\right)^2}\left(1-\left|\frac{q_z}{W_z}\right|\right)dq_z = \frac{\chi_N}{\kappa_{[011]}^2\left[1+\left(\frac{q_x}{\kappa_{[100]}}\right)^2+\left(\frac{q_y}{\kappa_{[011]}}\right)^2\right]^{3/2}}\tan^{-1}\left\{\frac{W_z}{\kappa_{[011]}^2}\frac{1}{\left[1+\left(\frac{q_x}{\kappa_{[100]}}\right)^2+\left(\frac{q_y}{\kappa_{[011]}}\right)^2\right]}\right\}. \tag{A2}$$

*Present address: Department of Physics, Tohoku University, Sendai 980-77, Japan.

[1] H. Unoki and T. Sakudo, J. Phys. Soc. Jpn. **23**, 546 (1967); P. A. Fleury, J. F. Scott, and J. M. Worlock, Phys. Rev. Lett. **21**, 16 (1968).

[2] G. Shirane and Y. Yamada, Phys. Rev. **177**, 858 (1969); R. A. Cowley, W. J. L. Buyers, and G. Dolling, Solid State Commun. **7**, 181 (1969).

[3] P. W. Anderson, in *Fizika Dielectrikov*, edited by G. I. Skanavi (Academy of Sciences, USSR, Moscow, 1960); W. Cochran, Adv. Phys. **9**, 387 (1960); R. A. Cowley, Phys. Rev. **134**, A981 (1964).

[4] A. D. Bruce and R. A. Cowley, *Structural Phase Transitions* (Taylor & Francis, London, 1981).

[5] T. Riste, E. J. Samuelson, K. Otnes, and J. Feder, Solid State Commun. **9**, 1455 (1971).

[6] S. M. Shapiro, J. D. Axe, G. Shirane, and T. Riste, Phys. Rev. B **6**, 4332 (1972).

[7] K. Gesi, J. D. Axe, and G. Shirane, Phys. Rev. B **5**, 1933 (1972).

[8] J. K. Kjems, G. Shirane, K. A. Müller, and H. J. Scheel, Phys. Rev. B **8**, 1119 (1973).

[9] J. D. Axe and G. Shirane, Phys. Rev. B **8**, 1965 (1973).

[10] J. B. Hastings, S. M. Shapiro, and B. C. Frazer, Phys. Rev. Lett. **40**, 237 (1978).

[11] R. Currat, K. A. Müller, W. Berlinger, and F. Denoyer, Phys. Rev. B **17**, 2937 (1978).

[12] B. I. Halperin and C. M. Varma, Phys. Rev. B **14**, 4030 (1976).

[13] R. A. Cowley and G. J. Coombs, J. Phys. C **6**, 143 (1973).

[14] S. R. Andrews, J. Phys. C **19**, 3721 (1986).

[15] D. F. McMorrow, N. Hamaya, S. Shimomura, Y. Fujii, S. Kishimoto, and H. Iwasaki, Solid State Commun. **76**, 443 (1990).

[16] T. W. Ryan, R. J. Nelmes, R. A. Cowley, and A. Gibaud, Phys. Rev. Lett. **56**, 2704 (1986); A. Gibaud, T. W. Ryan, and R. J. Nelmes, J. Phys. C **20**, 3833 (1987).

[17] T. R. Thurston, G. Helgesen, Doon Gibbs, J. P. Hill, B. D. Gaulin, and G. Shirane, Phys. Rev. Lett. **70**, 3151 (1993).

[18] T. R. Thurston, G. Helgensen, J. P. Hill, Doon Gibbs, B. D. Gaulin, and P. J. Simpson, Phys. Rev. B **49**, 15 730 (1994).

[19] P. M. Gehring, K. Hirota, C. F. Majkrzak, and G. Shirane, Phys. Rev. Lett. **71**, 1087 (1993).

[20] K. Hirota, G. Shirane, P. M. Gehring, and C. F. Majkrzak, Phys. Rev. B **49**, 11 967 (1994).

[21] P. M. Gehring, K. Hirota, C. F. Majkrzak, and G. Shirane, Phys. Rev. B **51**, 3234 (1995).

[22] G. Shirane, R. A. Cowley, M. Matsuda, and S. M. Shapiro, Phys. Rev. B **48**, 15 595 (1993).

[23] Sanders Associates, Electro-Optics Div., 95 Canal St., Nashua, NH 03060.

[24] Atomergic Chemetals Co., 222 Sherwood Av., Farmingdale, NY 11735-1718.

[25] Earth Jewelry (now renamed to Earth Chemical Co., Inorganic Div.), 2-1-30, Hamabe-dori, Chuo-ku, Kobe 651, Japan.

[26] J. Schneider, J. E. Jørgensen, and G. Shirane, Phase Transitions **8**, 17 (1986).

[27] C. N. W. Darlington and D. A. O'Connor, J. Phys. C **9**, 3561 (1976).

[28] M. Kawasaki, K. Takahashi, T. Maeda, R. Tsuchiya, M. Shinohara, O. Ishiyama, T. Yonezawa, M. Yoshimoto, and H. Koinuma, Science **266**, 1540 (1994).

[29] G. Shirane, Rev. Mod. Phys. **46**, 437 (1974).

[30] A. Gibaud, H. You, S. M. Shapiro, and J. Y. Gesland, Phys. Rev. B **42**, 8255 (1990).

[31] H. B. Neumann, U. Rütt, J. R. Schneider, and G. Shirane, Phys. Rev. B **52**, 3981 (1995).
[32] Y. Imry and M. Wortis, Phys. Rev. B **19**, 3580 (1979).
[33] D. P. Osterman, K. Mohanty, and J. D. Axe, J. Phys. C **21**, 2635 (1988).
[34] T. C. Lubensky and M. H. Rubin, Phys. Rev. B **12**, 3885 (1975).
[35] J. D. Axe (private communication).
[36] A. Okazaki, N. Ohama, and K. A. Müller, J. Phys. C **19**, 5019 (1986).
[37] R. A. Cowley (unpublished).
[38] Q. J. Harris, Q. Feng, R. J. Birgeneau, K. Hirota, K. Kakurai, J. E. Lorenzo, G. Shirane, M. Hase, K. Uchinokura, H. Kojima, I. Tanaka, and Y. Shibuya, Phys. Rev. B **50**, 12 606 (1994).
[39] G. M. Watson, B. D. Gaulin, T. R. Thurston, Doon Gibbs, P. J. Simpson, and G. H. Lander (unpublished).